THE JOURNAL OF PHYSICAL CHEMISTRY A

Subscriber access provided by UNIV OF ALABAMA BIRMINGHAM

A: Spectroscopy, Molecular Structure, and Quantum Chemistry

Valence and Inner Electronic Excitation, Ionization and Fragmentation of Perfluoropropionic Acid

Yanina Berrueta Martínez, Yanina Belén Bava, Reinaldo Luiz Cavasso Filho, Mauricio Federico Erben, Rosana Mariel Romano, and Carlos Omar Della Védova

J. Phys. Chem. A, **Just Accepted Manuscript** • DOI: 10.1021/acs.jpca.8b09252 • Publication Date (Web): 22 Nov 2018

Valence and Inner Electronic Excitation, Ionization and Fragmentation of Perfluoropropionic Acid

Yanina Berrueta Martínez,[ξ] Yanina B. Bava,[ξ] Reinaldo L. Cavasso Filho, [β] Mauricio F. Erben,[ξ] Rosana M. Romano,[ξ,*] and Carlos O. Della Védova[ξ,*]

[ξ]CEQUINOR (UNLP-CONICET-CIC), Departamento de Química, Facultad de Ciencias Exactas, Universidad Nacional de La Plata, 47 esq. 115, 1900 La Plata, República Argentina

[β]Universidade Federal do ABC, Rua Catequese, 242, CEP: 09090-400, Santo André, São Paulo, Brazil

Abstract

The photoexcitation, photoionization and photofragmentation of gaseous $CF_3CF_2C(O)OH$ were studied by means of synchrotron radiation in the valence and inner energy regions.

Photofragmentation events were detected from 11.7 eV through formation of COH^+, $C_2F_4^+$ and the parent species M^+. Since the vertical ionization potential has been reported at 11.94 eV, the starting energy used in this study, 11.7 eV, falls just inside the tale of the ionization band in the photoelectron spectra.

The information from the Total Ion Yield spectra around the C 1s, O 1s and F 1s ionization potentials allows the energies at which different resonance transitions take place in the molecule to be determined. These transitions have been assigned by comparison with the results of the analysis of similar compounds. In the inner energy region both kinetic energy release (KER) values and the slope and shape of double coincidence islands obtained from PhotoElectron-PhotoIon-PhotoIon-Coincidence (PEPIPICO) spectra allow different photofragmentation mechanisms to be elucidated.

*Corresponding authors email address: romano@quimica.unlp.edu.ar and carlosdv@quimica.unlp.edu.ar

Introduction

Fluoro- and perfluoro-organic compounds have found a wide variety of applications. As a result, particular representatives of this family, namely the perfluorocarboxylic acids, are spread throughout the environment; they have been found in human and animal tissues,[1] wastewater plants,[2] environmental waters[3,4] and in the atmosphere.[5,6] Their bioaccumulation[7,8] and environmental persistence, along with their potentially harmful nature for animals, including humans, have caused attention to be focused on them as a chemical family, mainly in the last decade.[9,10,11,12]

Ellis and coworkers studied the atmospheric degradation of fluorotelomer alcohols as a likely source of perfluorinated carboxylic acids in the environment.[13] Moreover, Andersen et al. reported another reaction path, between $C_2F_5C(O)O_2$ and HO_2, that would explain, at least in part, the presence of perfluorinated acids in the environment.[14]

Sekiguchi and coworkers have already used sonochemical methods and UV irradiation to study the effect of the degradation of hydrophobic perfluoroctane.[15] In a related way, Li and coworkers have used nanoparticles of modified TiO_2 to decompose an emerging pollutant, perfluorooctanoic acid.[16]

Perfluoropropionic acid, $CF_3CF_2C(O)OH$ (PFPA), may not accumulate to the same extent as the longer chain perfluorinated carboxylic acids;[7,8] neither have its natural sources been identified so far. That it has been detected in rainwater,[17,18,19] however, stresses its role as an environmentally active molecule.

Our research group has been involved for many years in photochemical studies of very simple species, using both non-ionizing and ionizing radiation. Thus, the determination of photevolution mechanisms in a wide energy range became possible together with the detection of the involved intermediates.[20,21]

Here we present the results of a photolysis study of PFPA using a wide range of synchrotron radiation extending from VUV to X-Ray in the electromagnetic spectrum. Valence (11.7–21.4 eV) and inner shell (278.0-750.0 eV) energies were investigated, as were Total Ion Yield (TIY), PhotoElectron-PhotoIon-Coincidence (PEPICO), and

PhotoElectron-PhotoIon-PhotoIon-Coincidence (PEPIPICO) spectra, in order to follow both excitation and ionization processes. From an analysis of these data, moreover, a number of fragmentation mechanisms were deduced.

Experimental section

The LNLS[22] facilities were used to perform the experiments detailed below. TGM and SGM beamlines were employed in two campaigns along with coincidence technique spectra. The experimental set-up has been previously described elsewhere.[23]

Perfluoropropionic acid 97 % was purchased from Sigma Aldrich and used as received.

The experiments were performed at the Brazilian Synchrotron Light Source (LNLS), located at Campinas, Brazil. For the low photon energy range, below 22 eV, we made use of the Toroidal Grating Monochromator (TGM) beamline. Although this is the oldest beamline in operation at LNLS, a relatively recent development was incorporated in the beamline, which makes it one of few vacuum ultraviolet beamlines with an efficient high harmonics filter.

For the soft X-ray region, we made use of the Spherical Gratting Monochromator (SGM) beamline, which provides photons with energies ranging from 250 eV to 1000 eV. The photons that come out from this beamline have an energy resolution $E/\Delta E$ in the order of 3000 and due to the mirrors reflection angles the high harmonics contamination is almost insignificant and can be completely dismissed for energies above 500 eV.
All the photoionization experiments were performed using a Wiley McLaren Time-of-Flight (TOF) mass spectrometer. In this mass spectrometer, following the photoionization process, the electrons and the positive ions are directed in opposite directions by static electric fields and collected by micro-channel plates. The sample is introduced in the chamber as an effusive beam. The electrons are detected without energy analysis and their electronic signals are the marker for the TOF spectrum. The software and the electronics allow us to perform multi-stop signal analysis, that is, one electron can be correlated to more than one ion fragment. In this way, we can analyze not only PhotoElectron-PhotoIon-

Coincidence (PEPICO) events, related to single ionic fragment production, but also PhotoElectron-PhotoIon-PhotoIon-Coincidence (PEPIPICO) events, where more than one ionic fragment is generated by only one photon. The time resolution of the TOF spectra are limited by the hardware that performs the time to digital conversion, with a resolution of 1 ns.

Computational calculations

The Gaussian 03 package[24] was used for all the quantum chemical calculations presented in this work. The optimizations of both neutral PFPA and cationic $PFPA^+$ were achieved using B3LYP/6-311+g(d) and UB3LYP/6-311+g(d) levels of approximation, respectively. A conformational search was performed for the neutral species by varying concurrently both O5-C2-O11-H12 and C4-C3-C2-O5 torsion angles. The conformer gauche-syn, gauche with respect to the C4-C3-C2-O5 and syn regarding the O5-C2-O11-H12 torsion angles, with a computed abundance of 85 % at room temperature, using the B3LYP/6-3111+g(d) approximation, will be selected for the further studies. The conformer syn-syn with an estimated abundance of 15 % at ambient temperature will not be further considered along this discussion. The molecular orbitals for the gauche-syn form were obtained from the optimized structure of PFPA by computing the NBO through the MP2 method along with the 6-311+g(d) basis set.

Results and discussion

Valence region

Several PEPICO spectra were measured around the reported first vertical ionization potential (11.94 eV).[25] The generation of ionic fragments in PEPICO spectra (Figure 1) at energies ranging between 11.7 and 11.8 eV − a little bit lower than the ionization potential of PFPA − can be explained by the fact that these values lie just inside the tale of the broad ionization band of the photoelectron spectrum. An autoionization process offers an alternative but plausible explanation for this behavior. [26,27] In the present case, such a secondary process would lead to electron emission by the decay of a highly excited neutral

system, followed by different processes giving COH^+, $C_2F_4^+$ and the parent species M^+ as distinctive events. This autoionization event would be initiated by the generation of a super-excited electronic state ($PFPA^{**}$) with an internal excitation energy that has been known in other cases even to exceed the first ionization potential.[28] Other conceivable photoevolution channels could occur via an adiabatic ionization mechanism followed by photofragmentation events. Although the adiabatic ionization potential of PFPA has not yet been established, a lower value than the reported vertical IP would be expected as a result of the significant changes in geometry likely to occur between the fundamental (PFPA) and the excited ionic ($PFPA^+$) species. Table S1 lists the computed geometry differences between both normal and ionized species. As already mentioned, the first band observed in the photoelectron spectrum[25] of PFPA occurs in the region of 12 eV. This process formally implies the removal of an oxygen lone pair (2p) electron through the supply of the ionization energy that is fairly well reproduced by our computations (Table S2). The parameters most affected (Figure S1) after ionization are the O11−C2 and C2−C3 bond distances, the O11−C2−O5 and C2−C3−C4 bond angles, and the O11−C2−C3−C4, O11−C2−C3−F6, O11−C2−C3−F7, C4−C3−C2−O5, F6−C3−C2−O5 and F7−C3−C2−O5 torsion angles, all of them closely related to the removal of the oxygen lone pair electron in the first ionization process of the species. These changes in the molecular geometry after ionization are consistent with the expected difference between the adiabatic and vertical ionization values.

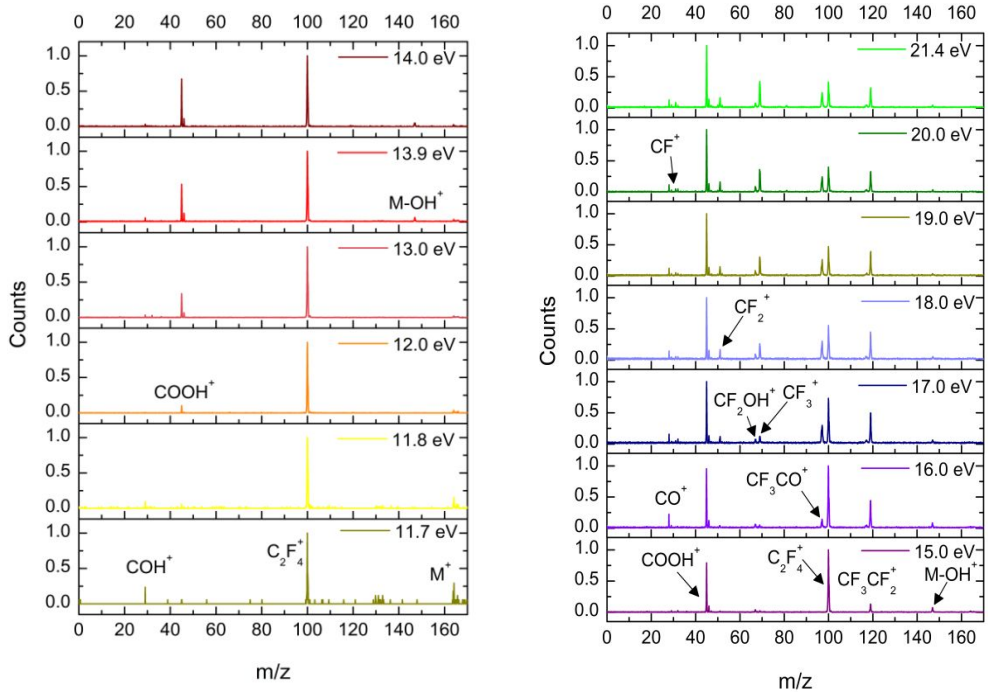

Figure 1. PEPICO spectra of PFPA taken in the valence energy region.

Three peaks can be observed in the spectrum collected at the lowest available energy at the LNLS (11.7 eV): the parent ion (M^+, m/z=164) in one process, and the fragments $C_2F_4^+$ (m/z=100) and COH^+ (m/z=29) as the products of two alternative photofragmentation channels. In the light of the increase of the C−C bond length of the CF_3CF_2−C(O)OH ionic species compared with the neutral molecule (Table S1), the events that leads to the formation of $C_2F_4^+$ on the one hand and COH^+ on the other hand through the rupture of the CF_3CF_2−C(O)OH bond are understandable.

Zha and coworkers studied in the gas phase the unimolecular photofragmentation of $CH_3C(O)OH$ and $CH_3C(O)OD$ in the electronic valence region (10.5-17.0 eV) using threshold photoelectron photoion coincidence mass spectrometry.[29] An ionic fragment corresponding to m/z=29, but *not* to m/z=30 in the case of $CH_3C(O)OD$, was observed, thereby excluding the formation of COH^+. The perfluorinated composition of PFPA and the existence of a fragment with m/z=29 indicates that its photofragmentation mechanism differs from that of acetic acid. Thus, the COH^+ fragment could be detected in the photofragmentation of PFPA. In order to confirm this new channel, complementary evidence is needed, however, before the existence of roaming mechanisms can be excluded.

At energies higher than the reported vertical ionization potential (about 12 eV) other photochannels become accessible. Thus a clear change in the fragmentation mechanisms is evidenced from the PEPICO spectra. The different photochannels that are evidenced by the increase in energy imply a decrease in the relative intensity of the already existing species at lower light beam energies. Here the intensity of the M^+ molecular ion and COH^+ fragment begins to decrease as the peak corresponding to the $COOH^+$ fragment (m/z=45) becomes significant. Starting at 15 eV, different fragmentation processes take place according to the results of these spectra. New fragments identified are $CF_3CF_2C(O)^+$, $CF_3CF_2^+$, CF_3CO^+, CO^+, CF^+, CF_2^+, CF_2OH^+, and CF_3^+.

Inner region

TIY spectra

Figure 2 presents C1s, O1s and F1s TIY spectra. All three spectra resemble the ISEEL spectra reported for $CF_3C(O)OH$ in the same energy regions.[30] The formal difference between $CF_3C(O)OH$ and $CF_3CF_2C(O)OH$, corresponds to the insertion of a $–CF_2–$ unit, so that good agreement is to be expected between the two spectra. For instance, the peak located at 288.0 eV in the TIY of PFPA corresponds to the C 1s → π*(C=O) resonance transition assigned by comparison with the 288.46 eV peak reported for $CF_3C(O)OH$[30] and the 287.4 eV peak in the TIY of $CF_3CF_2CF_2C(O)Cl$.[23]

When compared with $CF_3C(O)OH$, the chain elongation of PFPA provides more signals with the resultant overlapping of different peaks in the 292.0-300.0 eV energy region.[30] These absorptions emerge from resonance electronic transitions from C 1s to distinctive σ*(C−C) and σ*(C−F) molecular orbitals.

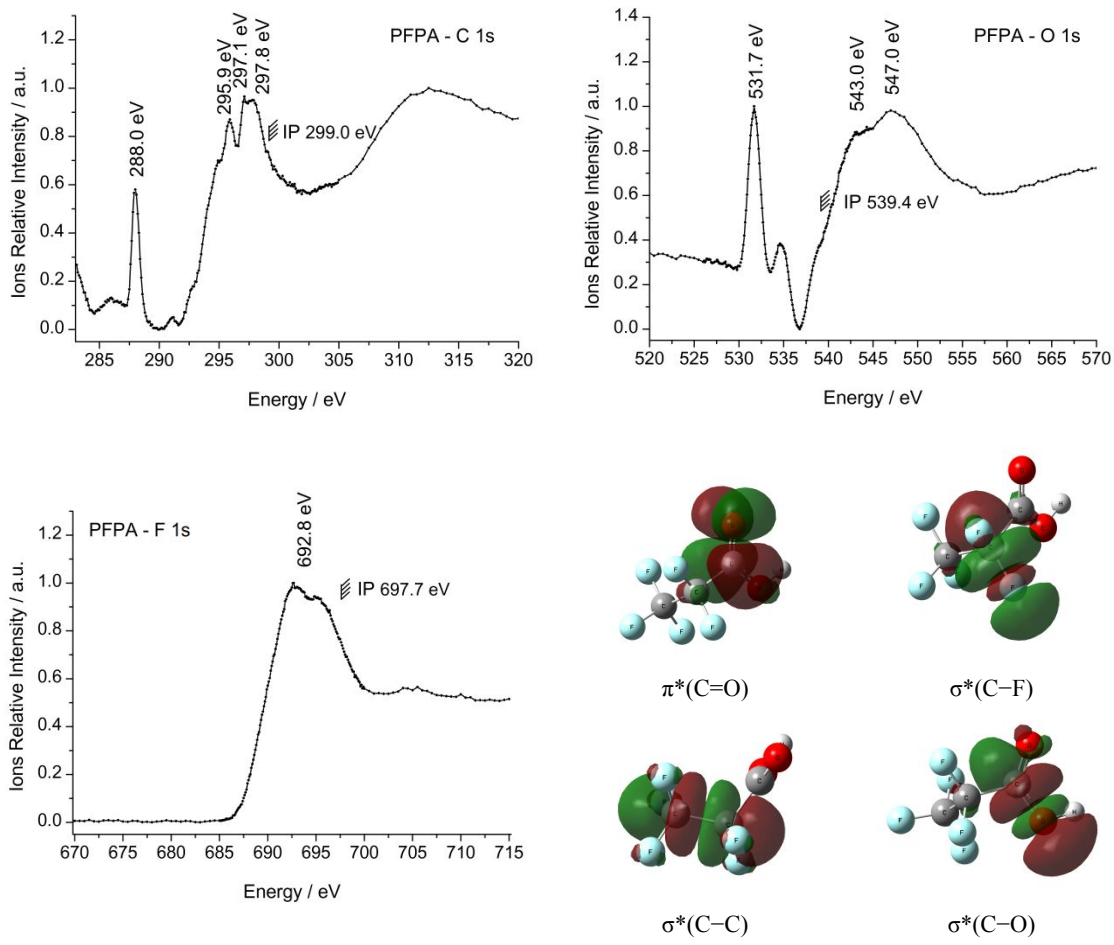

Figure 2. Total ion yield spectra of PFPA in the regions corresponding to the ionization of C 1s, O 1s and F 1s and some antibonding moelcular orbitals computed at the MP2/6-311+g(d) level of approximation.

The signal located at 531.7 eV is straightforwardly associated with a transition of an O 1s to π*(C=O) transition.[233] Moreover, the O 1s ionization potential is around 539 eV, similar to that in trifluoroacetic acid.[30] The higher energy absorptions at 543.0 and 547.0 eV (Figure 2) are assigned to Rydberg transitions from the O 1s orbital to oxygen Rydberg atomic orbitals of PFPA.[233]

The region of 695 eV, typical of a number of F 1s → σ *(C−F) resonance electronic transitions, appears congested, but its shape, determined by the proximity of several transitions, resembles that observed for other, related fluorine-containing molecules.[23] The F 1s ionization potential appears at 697.7 eV in PFPA (Figure 2).

PEPICO spectra

Photoelectron Photoion Coincidence spectra of PFPA were measured at 278.0, 288.0 (C 1s resonance), 299.0 (IP of C 1s), 340.0, 520.0, 531.7 (O 1s resonance), 539.4 (IP of O 1s), 590.0, 680.0, 692.8 (F 1s resonance), 697.7 (IP of F 1s) and 750.0 eV with the results depicted in Figure 3. Table 1 lists the evolution of the ionic fragmentations as a function of different energies. The general tendency is a growth in atomization processes at higher energies and the concomitant diminution of processes affording heavier fragments ($m/z \geq 45$). No clear behavior is detected for CF^+, CCF^+, CF_2^+, $C_2F_2^+$ and $C_2F_3^+$. They can be sourced by several different fragmentation mechanisms. Neither doubly charged ions nor specific fragmentations[31] were evidenced in the course of our experiments.

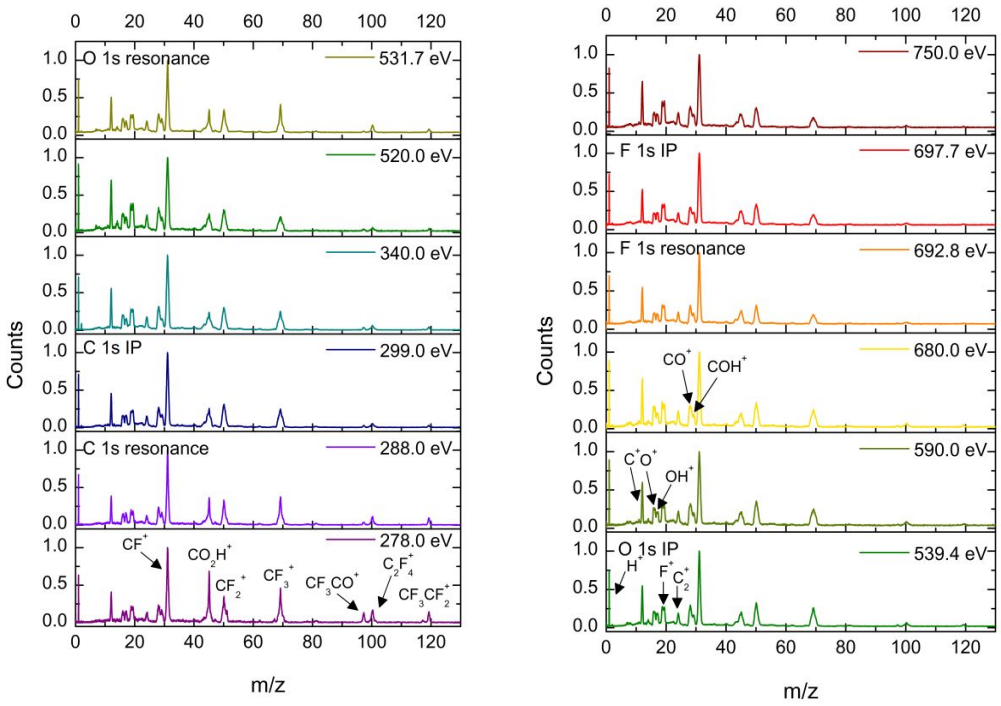

Figure 3. PEPICO spectra of PFPA taken at energies between 278 and 750 eV.

Table 1. PFPA branching ratios (%) in PEPICO spectra

m/z	Assignment	Energy / eV											
		278.0	288.0	299.0	340.0	520.0	531.7	539.4	590.0	680.0	692.8	697.7	750.0
1	H^+	5.95	6.21	6.59	6.13	7.61	6.73	7.34	7.87	8.17	6.85	6.58	7.37
12	C^+	8.06	8.16	8.75	10.21	12.31	9.98	10.69	10.77	11.59	11.64	10.32	12.55
16	O^+	4.25	4.74	4.34	4.61	9.89	6.56	5.94	7.32	5.59	6.06	5.76	6.47
17	OH^+	3.00	3.90	4.51	5.75	2.39	3.74	6.18	4.95	8.14	3.82	3.42	4.02

19	F^+	9.64	9.86	11.71	11.90	13.76	11.66	11.55	12.01	11.37	14.02	15.56	15.40
24	C_2^+	3.66	4.19	4.55	4.92	5.66	4.73	5.09	5.42	5.54	5.61	5.65	6.26
28	CO^+	5.76	5.81	6.58	7.05	6.80	5.78	6.46	7.02	6.94	6.19	5.96	6.45
29	COH^+	2.77	3.18	3.65	3.34	2.93	3.53	2.91	3.10	2.79	3.20	3.92	3.55
31	CF^+	21.63	23.03	23.17	22.04	20.01	21.28	21.54	20.21	19.83	23.72	23.17	21.49
43	CCF^+	2.34	1.86	1.46	1.55	2.24	2.56	2.33	2.31	2.20	2.41	1.31	1.67
45	$COOH^+$	10.39	7.57	7.71	7.40	4.59	5.79	4.69	4.38	4.04	5.35	5.89	4.72
50	CF_2^+	7.98	8.47	8.75	7.51	6.40	7.24	7.46	7.46	7.18	6.56	7.40	6.28
62	$C_2F_2^+$	0.14	0.25	0.24	0.21	0.14	0.20	0.32	0.22	0.00	0.22	0.32	0.14
69	CF_3^+	8.53	9.04	6.38	5.69	4.28	7.86	6.08	5.63	5.57	3.76	4.01	3.23
78	CF_2CO^+	0.18	0.20	0.08	0.13	0.00	0.13	0.00	0.00	0.00	0.00	0.00	0.00
81	$C_2F_3^+$	0.33	0.35	0.25	0.19	0.16	0.21	0.33	0.26	0.00	0.17	0.24	0.00
97	CF_3CO^+	1.30	0.37	0.20	0.28	0.16	0.11	0.11	0.08	0.09	0.00	0.06	0.00
100	$CF_2CF_2^+$	2.57	1.86	0.83	0.76	0.49	1.45	0.76	0.81	0.75	0.38	0.35	0.31
117	$CF_2CF_2OH^+$	0.25	0.00	0.05	0.06	0.00	0.00	0.00	0.00	0.00	0.00	0.00	0.00
119	$CF_3CF_2^+$	1.26	0.98	0.21	0.29	0.18	0.45	0.21	0.19	0.21	0.05	0.08	0.09

Fragmentation mechanisms

Kinetic energy release (KER)

KER values constitute an important source of information for establishing the mechanism of a given fragmentation. When the photolysis of a molecule produced by ionizing light occurs the charged species acquire a kinetic energy dependent on the formation process. The sum of the kinetic energies of the charged species formed in a given event expresses the KER of this process. Although the value of KER is a function of the properties of the ground state wave function of the molecule as well as the shape of the potential energy surfaces in which the charged species was formed, in the present case, the information of the KER will be used to contribute to the determination of the origin of the fragments observed in the PEPICO spectrum, that is, if they are a consequence of a photolysis process in which the precursor was simply or doubly charged. Experimentally this information can be collected from the analysis of the width of the TOF peak, which is proportional to the energy spread of the given charged fragment.

Table 2 lists a number of kinetic energy release values for cationic species originating in the fragmentation of PFPA at different incident energies and determined by analysis of their PEPICO spectra The fragments $CF_3CF_2^+$, $C_2F_4OH^+$, $C_2F_4^+$ and CF_3CO^+ present KER values close to the thermal energy (0.05 eV) for all the incident energies.[32] Fragments with energies lower than 0.20 eV are expected to be formed by fragmentation of singly charged ions, generating simultaneously neutral fragments that cannot be detected with our experimental setup.[33] Accordingly, the given charged fragment seems to be generated by the same mechanism at all energies. On the other hand, the KER values corresponding to the atomic fragments F^+, O^+, C^+ and H^+ and CF_2^+, CF^+, COH^+, CO^+, C_2^+ and OH^+ are higher than 0.20 eV at energies exceeding 278.0 eV, implying that these ions are produced by fragmentations involving at least one other ionic fragment (see next section). A combined analysis of the branching ratios and the KER values of the $C_2F_3^+$, CF_3^+ and $COOH^+$ fragments shows interesting results. The branching ratios reflect, in principle, not one but two fragmentation processes initiated in species either singly or doubly charged. For instance, the CF^+/CF_3^+ coincidence found in the PEPIPICO spectrum at higher energies confirms this hypothesis since both fragments must be derived from a doubly charged species (see next section, PEPIPICO spectra). However, the CF_3^+ fragment must come from singly charged fragments at lower energies since the KER values suddenly decrease from 0.28 eV at incident energy of 299 eV to 0.07 and 0.08 eV for incident energies of 278.0 and 288.0 eV, respectively. The fragment $COOH^+$ coincidentally shows a similar behavior.

Table 2. Kinetic Energy Release of cationic fragments of PFPA obtained by analysis of its PEPICO spectra taken at several incident energies (eV)

Assignment	Energy / eV											
	278.0	**288.0**	**299.0**	**340.0**	**520.0**	**531.7**	**539.4**	**590.0**	**680.0**	**692.8**	**697.7**	**750.0**
H^+	1.91	1.81	1.90	1.93	2.37	2.01	2.26	2.17	2.35	1.99	2.01	2.15
C^+	0.54	0.49	0.51	0.58	0.63	0.59	0.57	0.60	0.60	0.56	0.58	0.64
O^+	1.16	1.01	1.06	1.13	1.32	1.21	1.34	1.40	1.61	1.17	1.27	1.38
OH^+	0.61	0.57	0.79	0.72	1.10	0.71	1.09	0.99	0.93	0.69	0.69	0.84
F^+	1.78	1.92	1.56	1.62	2.04	1.95	1.98	1.86	1.84	1.65	1.67	1.84
C_2^+	0.42	0.38	0.35	0.35	0.40	0.37	0.38	0.38	0.42	0.35	0.39	0.39
CO^+	0.55	0.45	0.56	0.53	0.74	0.50	0.57	0.70	0.71	0.46	0.53	0.64
COH^+	0.31	0.33	0.48	0.62	0.51	0.39	0.48	0.44	0.47	0.40	0.50	0.49

CF^+	0.25	0.23	0.35	0.40	0.44	0.31	0.33	0.41	0.41	0.29	0.38	0.42
$COOH^+$	0.08	0.09	0.57	0.60	0.52	0.47	0.54	0.62	0.58	0.51	0.63	0.64
CF_2^+	0.32	0.21	0.35	0.37	0.39	0.29	0.30	0.36	0.36	0.28	0.37	0.37
CF_3^+	0.07	0.08	0.28	0.29	0.32	0.28	0.26	0.36	0.35	0.29	0.33	0.34
$C_2F_3^+$	0.09	0.07	0.08	0.14	0.06	0.05	0.17	0.20	0.12	0.00	0.06	0.00
CF_3CO^+	0.03	0.03	0.02	0.03	0.04	0.02	0.03	0.03	0.02	0.01	0.00	0.02
$C_2F_4^+$	0.03	0.04	0.09	0.05	0.10	0.04	0.11	0.14	0.14	0.14	0.10	0.07
$C_2F_4OH^+$	0.03	0.02	0.02	0.01	0.00	0.02	0.00	0.01	0.00	0.00	0.00	0.00
$CF_3CF_2^+$	0.02	0.02	0.02	0.02	0.02	0.02	0.02	0.04	0.03	0.02	0.02	0.01

PEPIPICO spectra

According to the formalism proposed by Eland, the relationship between the slope and the shape of a particular double coincidence island found in a PEPIPICO spectrum contains important information about the photofragmentation mechanism whereby both fragments are produced.[34,35] Since the collection of a PEPIPICO spectra is very time-consuming, the 697.7 eV region has been selected for thorough measurements. At this energy the coincidences involving H^+ ions in the PEPIPICO spectrum present without exception ovoid shapes which imply a concerted dissociation. The fragments C^+, CF^+ and CF_2^+ in coincidence with H^+ generate the most intense islands, that is, with a higher number of events. The remaining coincidence islands present parallelogram shapes with different slopes. Table 3 lists the parallelogram-shaped coincidences with their experimental slopes (Figure 4) and the proposed mechanisms suggested by the theoretical slopes.

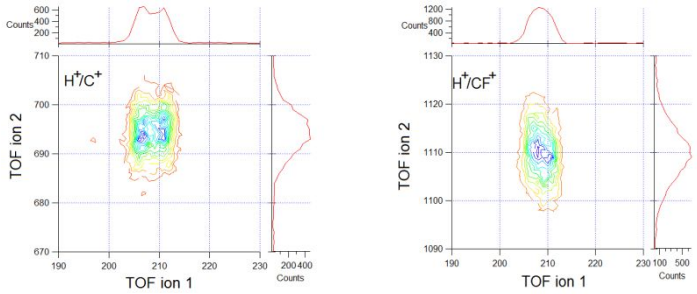

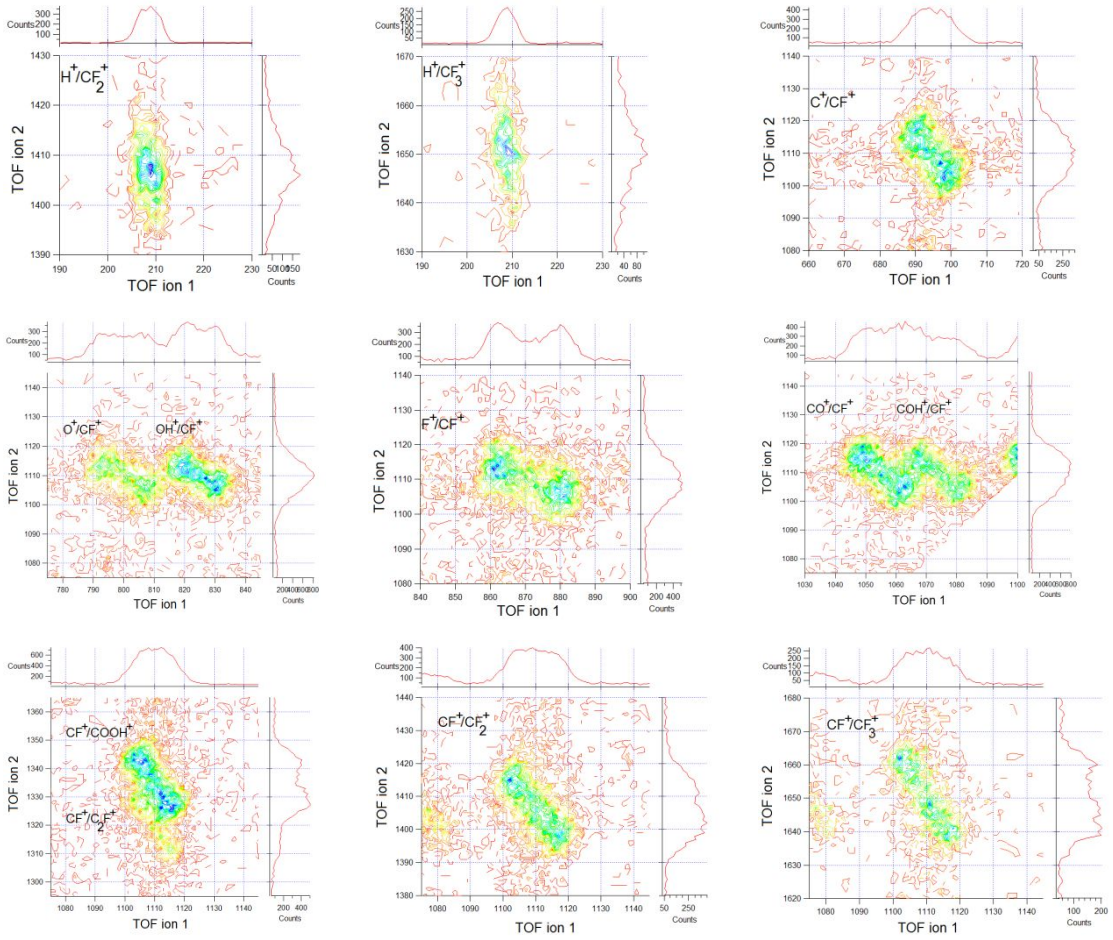

Figure 4. Selected coincidence islands for PFPA obtained at 697.7 eV.

Table 3. Experimental and theoretical slopes of different PEPIPICO parallelogram-shaped coincidence islands and the proposed mechanisms obtained at 697.7 eV following Eland´s formalism.

Coincidences	Experimental Slope[a)]	Theoretical Slope	Proposed Mechanism
O^+/CF^+	-0.71(1)	-0.72	SD-DCS
OH^+/CF^+	-0.69(10)	-0.62	SD-DCS
F^+/CF^+	-0.45(10)	-0.45	SD-DCS
CO^+/CF^+	-1.00(8)	-1.00	DCS
COH^+/CF^+	-0.99(8)	-1.00	DCS
$CF^+/COOH^+$	-1.61(8)	-1.61	SD-DCS
CF^+/CF_2^+	-1.06(8)	-1.00	DCS
CF^+/CF_3^+	-1.37(10)	-1.39	SD-DCS

SD-DCS: Secondary Decay after a Deferred Charge Separation, DCS: Deferred Charge Separation.

a) Values given in parentheses are 3 times standard deviations obtained from least-squares analysis.

All parallelogram-shaped coincidences correspond to Secondary Decay after Deferred Charge Separation (SD-DCS) and Deferred Charge Separation (DCS) fragmentation mechanisms, listed in Tables 4 and 5, respectively. It should be noted that the ionic fragments shown in bold are the only results provided by the experimental set-up used. Both experimentally non-observed neutral fragments and intermediate ionic species are assigned in agreement with the mechanism deduced from the experimental slope and the shape of the island.

We have already reported a COH^+/CF^+ coincidence in the photofragmentation of CF_3CH_2OH (TFE) at 294.5 eV. This island has an oval shape indicative of a concerted dissociation.[36] For PFPA the intensity of the COH^+/CF^+ coincidence island, with a slope of −0.99 and a parallelogram shape implying a Deferred Charge Separation according to Eland´s formalism, remains invariant at different energies. Thus, both CF_3CH_2OH and $CF_3CF_2C(O)OH$ produce the same photofragments but through different mechanisms.

Table 4. DCS mechanisms giving rise to CO^+/CF^+, COH^+/CF^+ and CF^+/CF_2^+ coincidence islands

Coincidence	DCS mechanism
CO^+/CF^+	$CF_3CF_2C(O)OH^{2+} \rightarrow CF_3 + CF_2C(O)OH^{2+}$
	$CF_2C(O)OH^{2+} \rightarrow F + O + H + CFCO^{2+}$
	$CFCO^{2+} \rightarrow \mathbf{CF^+} + \mathbf{CO^+}$
COH^+/CF^+	$CF_3CF_2C(O)OH^{2+} \rightarrow CF_3 + CF_2C(O)OH^{2+}$
	$CF_2C(O)OH^{2+} \rightarrow F + O + CFCOH^{2+}$
	$CFCOH^{2+} \rightarrow \mathbf{CF^+} + \mathbf{COH^+}$
CF^+/CF_2^+	$CF_3CF_2C(O)OH^{2+} \rightarrow CF_3CF_2^{2+} + C(O)OH$
	$CF_3CF_2^{2+} \rightarrow F + F + CF_2CF^{2+}$
	$CF_2CF^{2+} \rightarrow \mathbf{CF^+} + \mathbf{CF_2^+}$

Table 5. SD-DCS mechanisms giving rise to the O^+/CF^+, OH^+/CF^+, F^+/CF^+, $CF^+/C(O)OH^+$ and CF^+/CF_3^+ coincidence islands

Coincidence	SD-DCS mechanism
O^+/CF^+	$CF_3CF_2C(O)OH^{2+} \rightarrow CF_3 + F + OH + CFC(O)^{2+}$
	$CFC(O)^{2+} \rightarrow \mathbf{O^+} + CFC^+$
	$CFC^+ \rightarrow \mathbf{CF^+} + C$
OH^+/CF^+	$CF_3CF_2C(O)OH^{2+} \rightarrow CF_3 + CF_2C(O)OH^{2+}$

	$CF_2C(O)OH^{2+} \rightarrow \mathbf{OH^+} + CF_2C(O)^+$
	$CF_2C(O)^+ \rightarrow \mathbf{CF^+} + F + CO$
F^+/CF^+	$CF_3CF_2C(O)OH^{2+} \rightarrow CF_3CF_2^{2+} + C(O)OH$
	$CF_3CF_2^{2+} \rightarrow \mathbf{F^+} + CF_3CF^+$
	$CF_3CF^+ \rightarrow \mathbf{CF^+} + CF_3$
$CF^+/C(O)OH^+$	$CF_3CF_2C(O)OH^{2+} \rightarrow CF_3 + CF_2C(O)OH^{2+}$
	$CF_2C(O)OH^{2+} \rightarrow \mathbf{C(O)OH^+} + CF_2^+$
	$CF_3CF^{2+} \rightarrow \mathbf{CF^+} + CF_3$
CF^+/CF_3^+	$CF_3CF_2C(O)OH^{2+} \rightarrow CF_3CFC^{2+} + F + O + OH$
	$CF_3CFC^{2+} \rightarrow \mathbf{CF_3^+} + CFC^+$
	$CFC^+ \rightarrow \mathbf{CF^+} + F$

For a molecule with molecular weight 164, doubly ionized fragments that might be realized in the PEPICO spectra are limited to a value of m/z ≤ 82. Just one heaviest fragment is detected in the PEPICO spectra in this region, being therefore a candidate proceeding from a coulombic explosion, and this with a value of m/z = 81 corresponding to $C_2F_3^+$. Table 2 lists the KER behavior of this fragment which at 590 eV exhibits a KER value of 0.26, consistent with a doubly ionized precursor. There is no sign of its counterpart with m/z = 83 in the PEPIPICO spectra.

As already mentioned, ions with m/z > 82 must be generated from fragmentation of a singly charged ion. The fact that their KER values do not exceed 0.20 lends weight to this conclusion.

The photoevolution of PFPA gives the observed ionized and neutral species constituted, for instance, by fragments or molecules like CF_3, F, OH, O, F_2, C(O)OH, CF_2, C and H. After photolysis the recombination products formed in each case can lead to a number of long-lived fluoro- or perfluoro-chemicals made thermally and chemically stable by the strength of their C−F bonds.

Conclusions

The photoevolution of perfluoropropionic acid (PFPA) was studied under the influence of synchrotron radiation in the range from 11.7 to 715.0 eV. Photofragmentation events were

detected at the limit of the vertical ionization potential (11.94 eV)[255] corroborating the formation of COH^+, $C_2F_4^+$ and the parent M^+ ion. The evidence associated with the display of these fragments below the reported ionization potential might point to either auto- or adiabatic ionization. At much higher energies the TIY spectra around the C 1s, O 1s and F 1s levels were measured with results in total agreement with the previously reported TIY spectra of related fluorinated species. PEPICO spectra acquired at valence and inner energy regions are also presented in this work. The measured KER values in the higher energy region of the PEPICO spectra, along with the PEPIPICO spectra taken at 697.7 eV, allow us to elucidate different photofragmentation mechanisms. It should be noted that the study of the vibrational spectra of PFPA carried out by Crowder[37] establishes the partial association of this acid in the vapor phase. However, without being able positively to rule out a role for the dimer of PFPA in the interpretation of our experiments, all the signals reported here can be explained as originating in the monomer, the heaviest fragment to be detected being the parent M^+ ion at 164 m/z.

Acknowledgement

The authors are especially grateful to Prof. Dr. Anthony J. Downs of the University of Oxford, who, due to his infinite generosity, preferred to share this work enlightened by his knowledge from this position.

The work described in this paper is based on the experiments performed at the Laboratório Nacional de Luz Síncrotron (LNLS) under the proposals TGM-15163 and SGM-17920. We would like to thank the LNLS institution and their staff for accepting our proposals and for helping us during our measurements. We also thank the Facultad de Ciencias Exactas of the Universidad Nacional de La Plata and Consejo Nacional de Investigaciones Científicas y Técnicas (CONICET) for the financial support. ANPCYT is also gratefully acknowledged for the grants PICT 2014–2957 and PICT 2017-3230.

Supporting information available:

This contains the computed parameters corresponding to the optimized structures of PFPA and $PFPA^+$ (Table S1), the 51 lowest energy molecular orbitals (MO) corresponding to PFPA calculated with the NBO MP2/6-311+g(d) approximation in its C_1 point group of symmetry (Table S2) and the atomic numbering of PFPA and $PFPA^+$ used in Table S1 (Figure S1).

References

1 Moody, C.A.; Martin, J.W.; Kwan, W.C.; Muir, D.C.G.; Mabury, S.A. Monitoring perfluorinated surfactants in biota and surface water samples following an accidental release of fire-fighting foam into Etobicoke Creek. *Environ. Sci. Technol.* **2002**, *36*, 545-551.

2 Zhang, C.; Yan, H.; Li, F.; Zhou, Q. Occurrence and fate of perfluorinated acids in two wastewater treatment plants in Shanghai, China. *Environ. Sci. Pollut. Res*. **2015**, *22*, 1804-1811.

3 Yamashita, N.; Kannan, K.; Taniyasu, S.; Horii, Y.; Petrick, G.; Gamo, T. A global survey of perfluorinated acids in oceans. *Mar. Pollut. Bull*. **2005**, *51*, 658-**6**68.

4 So, M.K.; Miyake, Y.; Yeung, W.Y.; Ho, Y.M.; Taniyasu, S.; Rostkowski, P. Perfluorinated compounds in the Pearl River and Yangtze River of China. *Chemosphere*. **2007**, *68*, 2085-2095.

5 Ellis, D.A.; Mabury, S.A.; Martin, J.W.; Muir, D.C.G. Thermolysis of fluoropolymers as a potential source of halogenated organic acids in the environment. *Nature*. **2001**, *412*, 321-324.

6 Tian, Y.; Yao, Y.; Chang, S.; Zhao, Z.; Zhao, Y.Y.; Yuan, X.J.; Wu, F.C.; Sun, H.W. Occurrence and phase distribution of neutral and ionizable per- and polyfluoroalkyl substances (PFASs) in the atmosphere and plant leaves around landfills: a case study in Tianjin, China. *Environ. Sci. Technol.* **2018,** *52*, 1301-1310.

7 Martin, J.W.; Mabury, S.A.; Solomon, K.R.; Muir, D.C.G. Dietary accumulation of perfluorinated acids in juvenile rainbow trout (Oncorhynchusmykiss). *Environ. Tox. Chem.* **2003**, *22*, 189-195.

8 Martin, J.W.; Mabury, S.A.; Solomon, K.R.; Muir, D.C.G. Bioconcentration and tissue distribution of perfluorinated acids in rainbow trout (Oncorhynchusmykiss). *Environ. Tox. Chem*. **2003**, *22,* 196-204.

9 U.S. Environmental Protection Agency. Preliminary risk assessment of the developmental toxicity associated with exposure to perfluorooctanoic acid and its salts. Office of Pollution Prevention and Toxics, Risk Assessment Division, **2003**.

10 Berthiaume, J.; Wallace, K.B. Perfluorooctanoate, perflourooctanesulfonate, and N-ethyl perfluorooctanesulfonamido ethanol; peroxisome proliferation and mitochondrial biogenesis.*Toxicol.Lett.* **2002**, *129*, 23-32.

11 Upham, B.L.; Deocampo, N.D.; Wurl, B.; Trosko, J.E.. Inhibition of gap junctional intercellular communication by perfluorinated fatty acids is dependent on the chain length of the fluorinated tail. *Int. J. Cancer.* **1998,** *78*, 491-495.

12 Biegel, L.B.; Hurtt, M.E.; Frame, S.R.; Connor, J. O.; Cook, J.C. Mechanisms of extrahepatic tumor induction by peroxisome proliferators in male CD rats. *Toxicol. Sci.* **2001**, *60*, 44-55.

13 Ellis, D. A.; Martin, J. W.; De Silva, A. O.; Mabury, S. A.; Hurley, M. D.; Sulbaek Andersen, M. P.; Wallington, T. J. Degradation of fluorotelomer alcohols: a likely atmospheric source of perfluorinated carboxylic acids. *Environ. Sci. Technol*. **2004**, *38*, 3316-3321.

14 Sulbaek Andersen, M. P.; Hurley, M. D.; Wallington, T. J.; Ball, J. C.; Martin, J. W.; Ellis, D. A.; Mabury, S. A. Atmospheric chemistry of C_2F_5CHO: mechanism of the $C_2F_5C(O)O_2 + HO_2$ reaction. *Chem. Phy. Lett.* **2003**, *381*, 14-21.

15 Sekiguchi, K.; Kudo, T.; Sankoda, K. Combined sonochemical and short-wavelength UV degradation of hydrophobic perfluorinated compounds. *Ultrason. Sonochem.* **2017,** *114,* 201-208.

16 Li, M.; Yu, Z.; Liu, Q.; Sun, L.; Huang, W. Photocatalytic decomposition of perfluorooctanoic acid by noble metallic nanoparticles modified TiO_2, *Chem. Eng. J.* **2016,** *286*, 232-238.

17 Jackson, D.A.; Young, C.J.; Hurley, M.D.; Wallington, T.J.; Mabury, S.A. Atmospheric degradation of perfluoro-2-methyl-3-pentanone: Photolysis, hydrolysis and hydration. *Environ Sci. Technol.* **2011**, *45*, 8030-8036.

18 Scott, B.F.; Spencer, C.; Mabury, S.A.; Muir, D.C.G. Poly and perfluorinated carboxylates in North American precipitation. *Environ. Sci. Technol*. **2006**, *40*, 7167-7174.

19 Young, C.J.; Hurley, M.l.D.; Wallington, T.J.; Mabury, S.A. Atmospheric chemistry of CF_3CF_2H and $CF_3CF_2CF_2CF_2H$: Kinetics and products of gas-phase reactions with Cl atoms and OH radicals, infrared spectra, and formation of perfluorocarboxylic acids. *Chem. Phys. Lett.* **2009**, *473*, 251-256.
20 Moreno Betancourt A.; Bava Y.B.; Berrueta Martínez, Y.; Erben, M.F.; Cavasso Filho, R.L.; Della Védova, C.O. Photofragmentation mechanisms of chlorosulfonyl isocyanate, $ClSO_2NCO$, excited with synchrotron radiation between 12 and 550 eV. *J. Phys. Chem. A*. **2015**, *119*, 8021-8030.
21 Rodríguez Pirani, L.S.; Della Védova, C.O.; Geronés, M.; Romano, R.M.; Cavasso Filho, R.L.; Ge, M.F.; Ma, Ch. P.; Erben, M.F. Electronic properties and dissociative photoionization of thiocyanates, Part III. The effect of the group's electronegativity in the valence and shallow-core (sulfur and chlorine 2p) regions of CCl_3SCN and CCl_2FSCN. *J. Phys. Chem. A,* **2017**, *141*, 9201-9210.
22 Craievich, A. F.; Rodrigues, A. R. The Brazilian Synchrotron Light Source. *Hyperfine Interact*. **1998**, *113*, 465-475.
23 Berrueta Martínez, Y.; Bava, Y.B.; Erben, M.F.; Cavasso Filho, R.L.; Romano, R.M.; Della Védova, C.O. Photoexcitation, Photoionization, and photofragmentantion of $CF_3CF_2CF_2C(O)Cl$ using synchrotron radiation between 13 and 720 eV. *J. Phys. Chem. A*. **2015**, *119*, 1894-1905.
24 Frisch, M. J.; Trucks, G. W.; Schlegel, H. B.; Scuseria, G. E.; Robb, M. A.; Cheeseman, J. R.; Montgomery, Jr., J. A.; Vreven, T.; Kudin, K. N.; Burant et al. Gaussian 03, rev C.02; Gaussian, Inc.; Wallingford, CT, 2004.
25 Utsunomiya, C.; Kobayashi, T.; Nagakura, S. Photoelectron spectra of hydrogen-bonded complexes. *Bull. Chem. Soc. Jap.* **1979**, *52*, 3223-3225.
26 Brei-Im, B.; Fuchs V.; Kebarle, P. Autoionization and fragmentation processes in methanol and ethanol. *Int. J. Mass Spect. Ion Phys.* **1971**, *6*, 279-289.
27 Dujardin, G.; Leach, S.; Dutuit, O.; Govers, T.; Guyon, P.M. Autoionization processes in *syn*-trifluorobenzene and hexafluorobenzene: Studies involving threshold photoelectrons and ion fluorescence.*J. Chem. Phys*. **1983**, *79*, 644-657.
28 Lee, W.Y.; Lee, W.B.; Fu, H.; Pan, C.C.; Lin K.C. Ionization and dissociation mechanisms of ketene using resonance-enhanced multiphoton ionization mass spectrometer: (2+2) versus (2+1) schemes. *J. Chem. Phys.* **2001**, *115*, 7429-7435.
29 Zha, Q.; Nishimura, T.; Bertrand, M. J.; Meisels, G. G. Fragmentation of acetic acid ions with selected internal energies. *Intern. J. Mass Spectrom. Ion Proc.* **1991**, *107*, 515-529.
30 Robin, M. B.; Ishii, I.; McLaren, R.; Hitchkcoock, A. P. Fluorniation effects on the inner-shell spectra of unsaturated molecules. *J. Electron Specrosc. Relat. Phenom.* **1988**, *47*, 53-92.
31 Habenicht, W.; Baiter, H.; Müller-Dethlfs, K.; Sclag, E. W. Memory effects[22] in molecular fragmentation induced by site-specific core excitation using a reflectron time-of-flight mass spectrometer. *J. Phys. Chem.* **1991**, *95*, 6774-6780.
32 Santos, A. C. F.; Lucas, C. A.; de Souza, G. G. B. Dissociative photoionization of SiF_4 around the Si 2p edge: a new TOFMS study with improved mass resolution. *J. Electron Spectrosc. Relat.Phenom.* **2001**, *114-116*, 115-121.
33 Cortés, E.; Della Védova, C.O.; Geronés, M.; Romano, R.M.; Erben, M.F. Perchloromethyl mercaptan, CCl_3SCl, excited with synchrotron radiation in the proximity of the sulfur and chlorine 2p edges: Dissociative photoionization of highly halogenated species. *J. Phys. Chem. A*. **2009**, *113*, 9624-9632.
34 Eland, J. H. A new two-parameter mass spectrometry. *Acc. Chem. Res.* **1989**, *22*, 381-387.
35 Simon, M.; Lebrun, T.; Martins, R.; de Souza, G. G. B.; Nenner, I.; Lavollee, M.; Morin, P. Multicoincidence mass spectrometry applied to hexamethyldisilane excited around the silicon 2p edge. *J. Phys. Chem.* **1993**, *97*, 5228-5237.

36 Bava, Y.B.; Berrueta Martínez, Y.; Moreno Betancourt, A.; Erben, M.F.; Cavasso Filho, R.L.; Della Védova, C.O.; Romano, R.M. Ionic fragmentation mechanisms of 2,2,2-trifluoroethanol following excitation with synchrotron radiation. *ChemPhysChem*. **2015**, *16*, 322-330.
37 Crowder, G.A. Infrared and Raman spectra of pentafluoropropionic acid. *J. Fluorine Chem.* **1972**, *1*, 385-389.

TOC Graphic

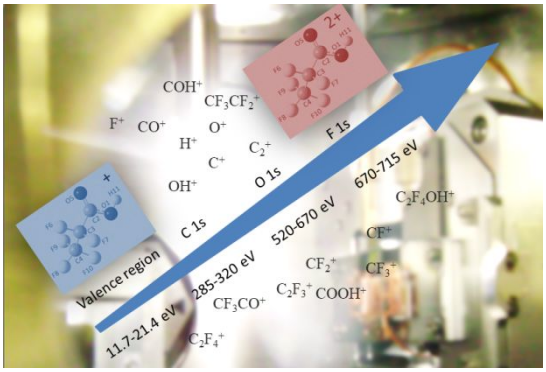
COH+
CF3CF2+
F+
CO+
O+
H+
C2+
C+
OH+
F 1s
O 1s
C 1s
670-715 eV
520-670 eV
285-320 eV
Valence region
11.7-21.4 eV
C2F4OH+
CF+
CF2+
CF3+
C2F3+ COOH+
CF3CO+
C2F4+